Supporting Information

Porous and amorphous cobalt hydroxysulfide core-shell nanoneedles on Ti-mesh as bifunctional electrocatalyst for energy-efficient hydrogen production via urea electrolysis

Yu Jiang,[a] *Shanshan Gao,*[*a,c] *Gongchen Xu,*[a] *and Xiaoming Song*[*a,b]

[a] Qingdao University of Science and Technology, Qingdao 266042, PR China

[b] State Key Laboratory of Biobased Material and Green Papermaking, Qilu University of Technology, Shandong Academy of Sciences, Jinan 250353, PR China

[c] Guangxi Key Laboratory of Clean Pulp & Papermaking and Pollution Control, Nanning 530004, PR China

E-mail: jyu4341@163.com; xiaomingsong4007@163.com (Xiaoming Song). □ Corresponding authors.

Materials

Cobalt (II) nitrate hexahydrate ($Co(NO_3)_2·6H_2O$), Urea (CH_4N_2O), Ammonium fluoride (NH_4F), Sodium sulfide nonahydrate ($Na_2S·9H_2O$), Potassium hydroxide (KOH), Ethanol absolute were supplied from Sinopharm Chemical Reagent Co. Ltd (www.sinoreagent.com). Pt/C (20%) and RuO_2 (99.9%) were purchased from Shanghai Macklin Biochemical Co., Ltd (Shanghai, China).

Preparation of $Co(CO_3)_{0.5}(OH)·0.11H_2O$ NN/Ti (CCH NN/Ti)

CCH NN/Ti was synthesized by a simple solvothermal method. First, 0.875 g $Co(NO_3)_2·6H_2O$, 0.60 g urea, 0.08 g NH_4F were dissolved into 20 mL deionized water to provide a uniform solution. Then the solution was transferred into a 50 mL autoclave lined with Teflon. The cleaned Ti-mesh was dipped in the autoclave and heated it at 120°C for 8 hours. After the autoclave naturally cooled to room temperature. The obtained sample was thoroughly cleaned with ultrapure water and ethanol, and dried it at room temperature.

Preparation of P-$CoS_x(OH)_y$ NN/Ti

P-$CoS_x(OH)_y$ NN/Ti was obtained by immersing the precursor CCH NN/Ti in 20 ml 3.0 M Na_2S under constant stirring at room temperature for 24 h, then washed it three times with ultrapure water and absolute ethanol and dry it at room temperature. The control experiments were carried out by controlling the concentrations of Na_2S for 1 M and 5 M, named as 1 M-NN and 5 M-NN, respectively. Moreover, the effect of different temperature conditions (room temperature, 100 ℃, 120 ℃, 140 ℃) on the catalyst was also studied. The mass loading of P-$CoS_x(OH)_y$ NN/Ti is about 3.2 mg cm^{-2}.

Characterizations

The X-ray diffraction (XRD) pattern was recorded on a Rigaku Ultima IV diffractometer (CuKα radiation, λ, = 1.5406Å) with an angle range of 5 to 90° with a scan rate of 5° min^{-1}. The morphology and corresponding element mapping images of all samples were obtained on a field emission scanning electron microscope (FE-SEM, JEOL JSM-7800F). In addition, a transmission electron microscope (TEM, JEOL JEM-2100 F) was used to characterize the microstructure and energy dispersive X-ray analysis. XPS spectra were recorded using Thermo ESCALAB 250XI electronic spectrometer. The specific surface area and pore size distribution of the catalyst were measured at 77 K by using ASAP2020.

Electrochemical Analyses

The electrochemical measurements of the samples were conducted using CHI-760E electrochemical workstation at room temperature. The HER and UOR catalytic activities were tested using a three-electrode system in 1.0 M KOH with 0.5 M urea (PH=13.7). Using a graphite rod and an Hg/HgO electrode as the counter electrode and reference electrode, respectively. The prepared samples (0.5×0.5 cm^{-2}) were adopted as the working electrode. Polarization curves were obtained at a scan rate of 5 mV s^{-1}. All the measured potentials were calibrated to the reversible hydrogen electrode (RHE) using the following equation: $E_{RHE} = E_{Hg/HgO} + 0.098 + 0.059$ PH. It needs to be noted that all the linear sweep voltammetry (LSV) curves were reported with 90% iR compensation. The Tafel plots was obtained from LSV curves using the Tafel equation: $\eta = b \log j + a$ (j is the current density, b is the Tafel slope). For overall urea splitting, using P-$CoS_x(OH)_y$ NN/Ti as both the cathode and anode in a two-electrode system. Cyclic voltammograms (CV) were recorded in 1.0 M KOH and 0.5 M urea with different scan rates from 20 to 100 mV s^{-1} in the potential range of −0.2 V − −0.1 V (vs.RHE). EIS measurements were conducted with a scan rate of 5 mV s^{-1}. The frequency ranges from 1000 KHz to 0.01 Hz. For comparison, Pt/C and RuO_2 were coated on Ti-mesh with the same loading amount as the above samples. Specifically, 3.2 mg of Pt/C or RuO_2 was dispersed in 960 mL and 40 mL 5% Nafion, then the suspension was coated on Ti-mesh (1×1 cm^{-2}) and dried under ambient conditions. In addition, the prepared Pt/C or RuO_2 electrode on the Ti-mesh is cut into a size of 0.5×0.5 cm^{-2} and reserved for testing. All the electrochemical measurements were conducted at ambient temperature. A single AA battery (1.5 V) and commercial solar panel (6.0 V) are used to provide power the urea electrolysis process.

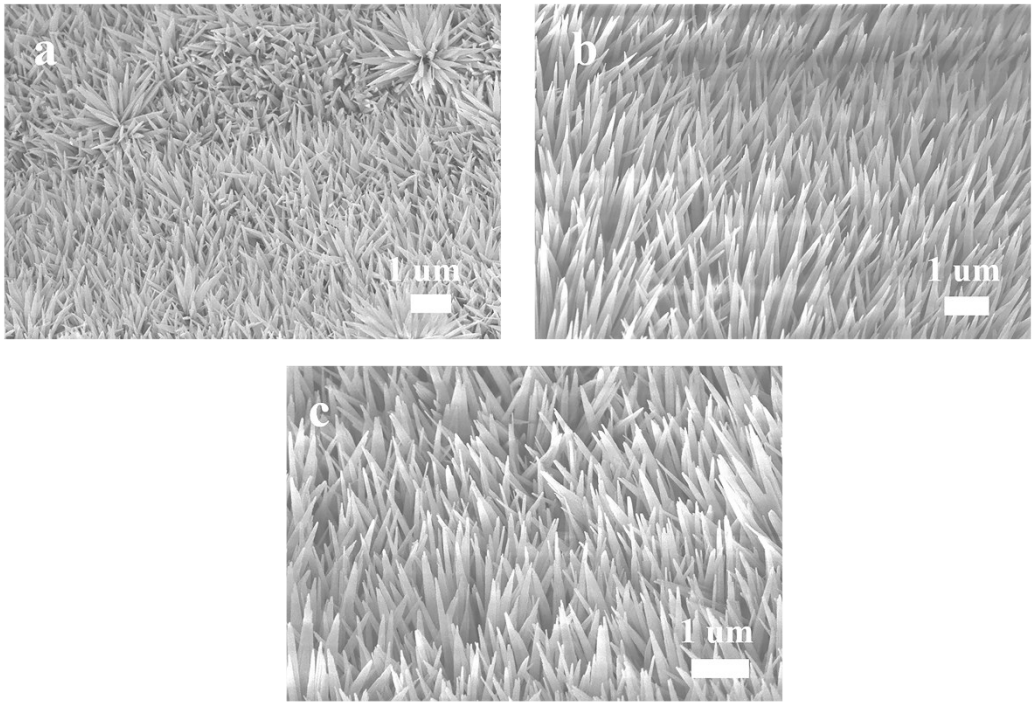

Figure S1. SEM images of $Co(CO_3)_{0.5}(OH)\cdot 0.11H_2O$ prepared under the reaction condition of 120 °C for different times (6 h (a), 8 h (b), 10 h (c)).

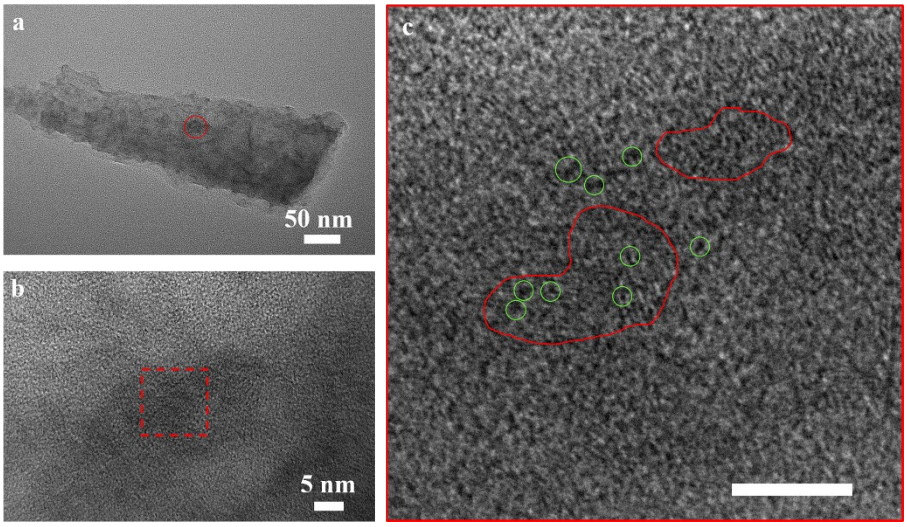

Figure S2. (a) TEM images of P-$CoS_x(OH)_y$ NN. (b) HR-TEM image of the core for P-$CoS_x(OH)_y$ NN. (c) Enlarged images of the HR-TEM (Red dotted area).

Figure S3. TEM images of P-$CoS_x(OH)_y$ NN/Ti.

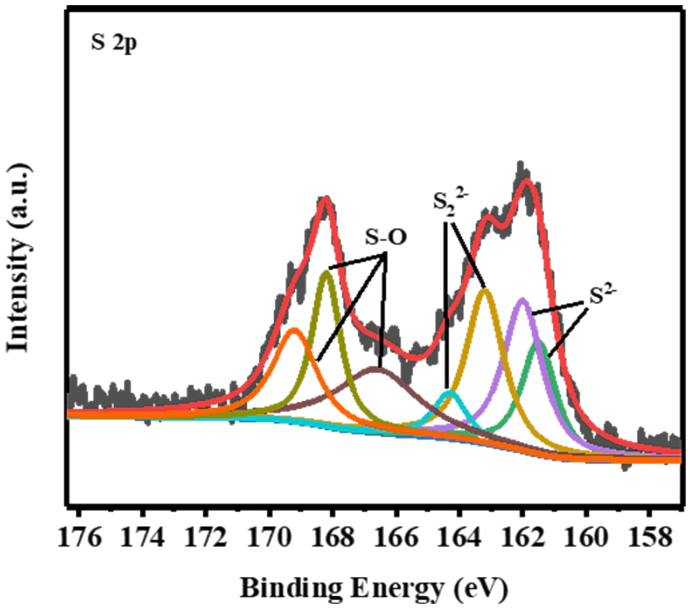

Figure S4. S 2p XPS curves of P-$CoS_x(OH)_y$ NN/Ti.

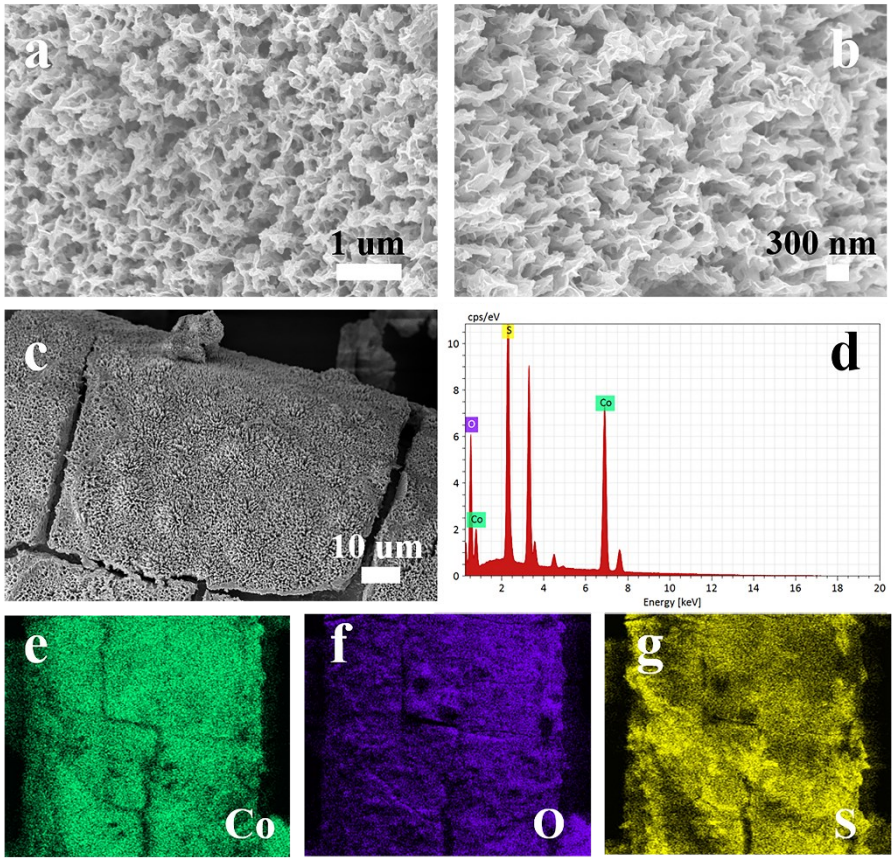

Figure S5. (a-c) SEM images, (d) EDX pattern and (e-g) SEM mapping of P-$CoS_x(OH)_y$ NN/Ti after long-term HER electrolysis.

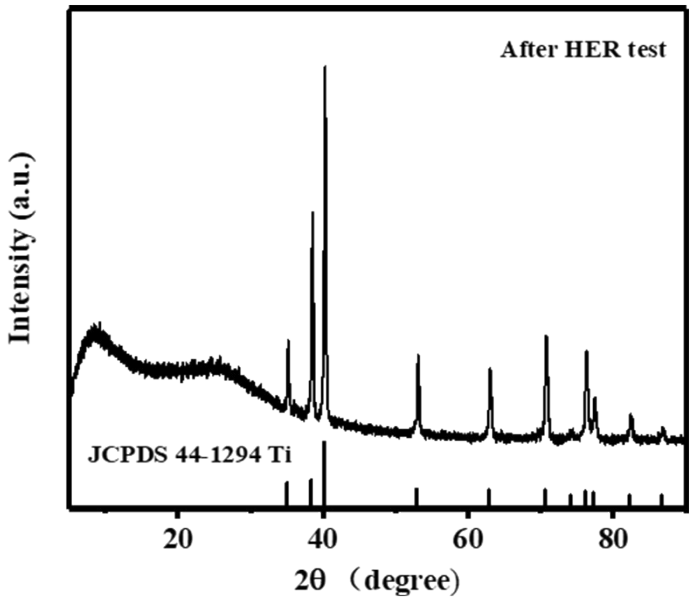

Figure S6. XRD patterns of P-$CoS_x(OH)_y$ NN/Ti after long-term HER electrolysis.

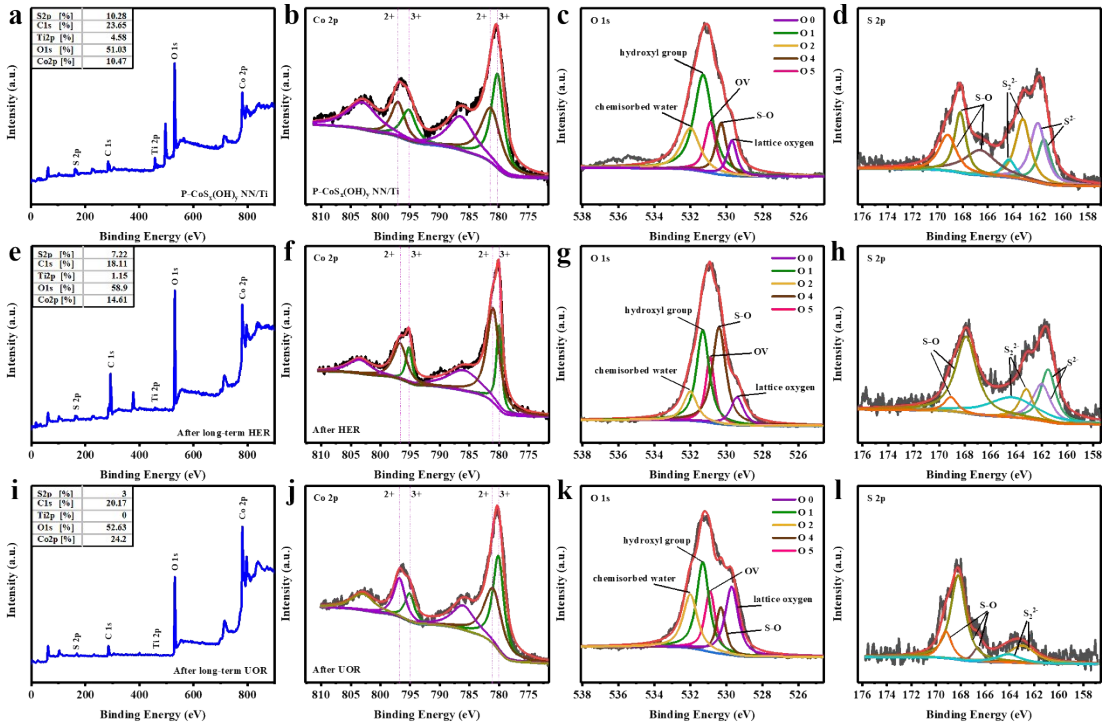

Figure S7. The full survey, Co2p, O1s and S2p XPS curves of P-$CoS_x(OH)_y$ NN/Ti (a~d), P-$CoS_x(OH)_y$ NN/Ti after long-term HER (e~h) and P-$CoS_x(OH)_y$ NN/Ti after long-term UOR (i~l), respectively. Note: the insert in the full survey is the Atomic content ratio of the S, C, Ti, O and Co calculated from the XPS.

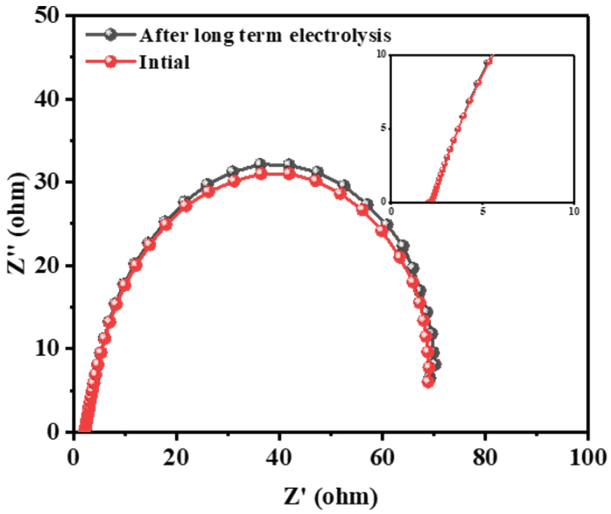

Figure S8. Nyquist plots of P-$CoS_x(OH)_y$ NN/Ti at the overpotential of 0.2 V before and after long-term electrolysis for HER.

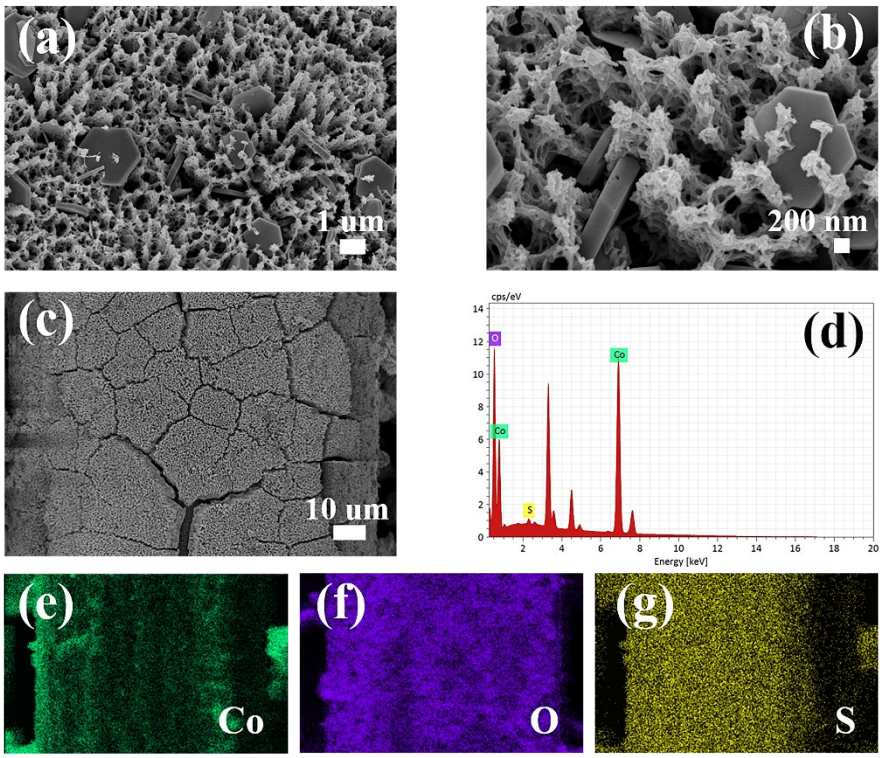

Figure S9. (a-c) SEM images, (d) EDX pattern and (e-g) SEM mapping of P-$CoS_x(OH)_y$ NN/Ti after long-term UOR electrolysis.

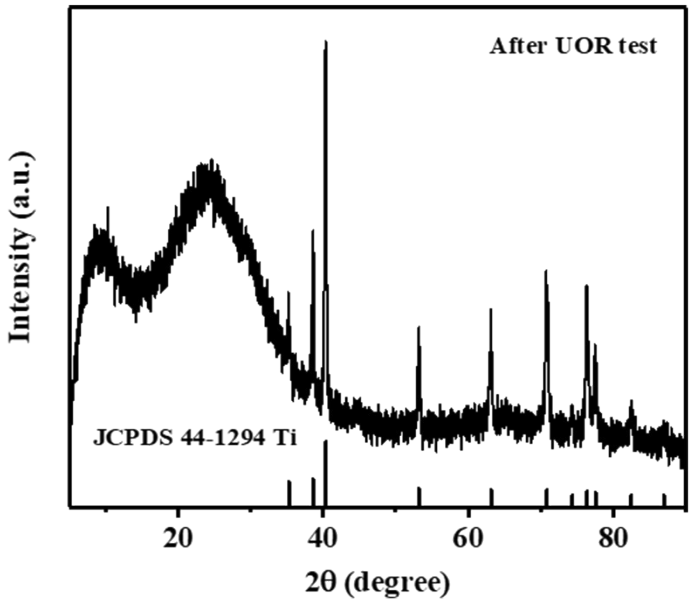

Figure S10. XRD patterns of P-$CoS_x(OH)_y$ NN/Ti after long-term UOR electrolysis.

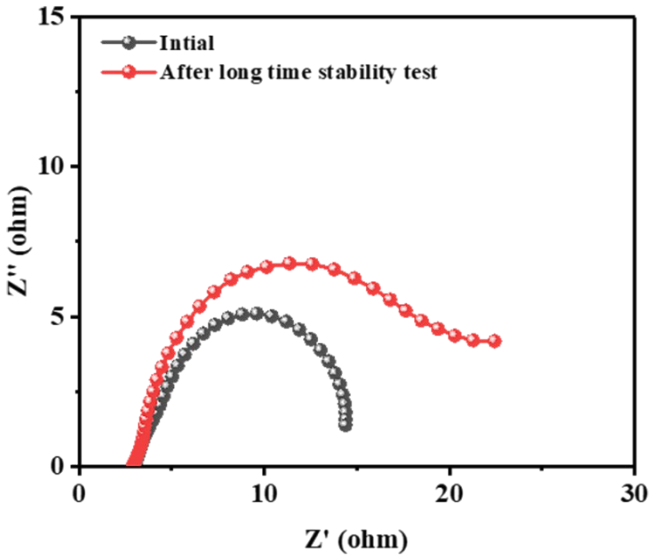

Figure S11. Nyquist plots of P-$CoS_x(OH)_y$ NN/Ti at the overpotential of 1.3 V before and after long-term electrolysis for UOR.

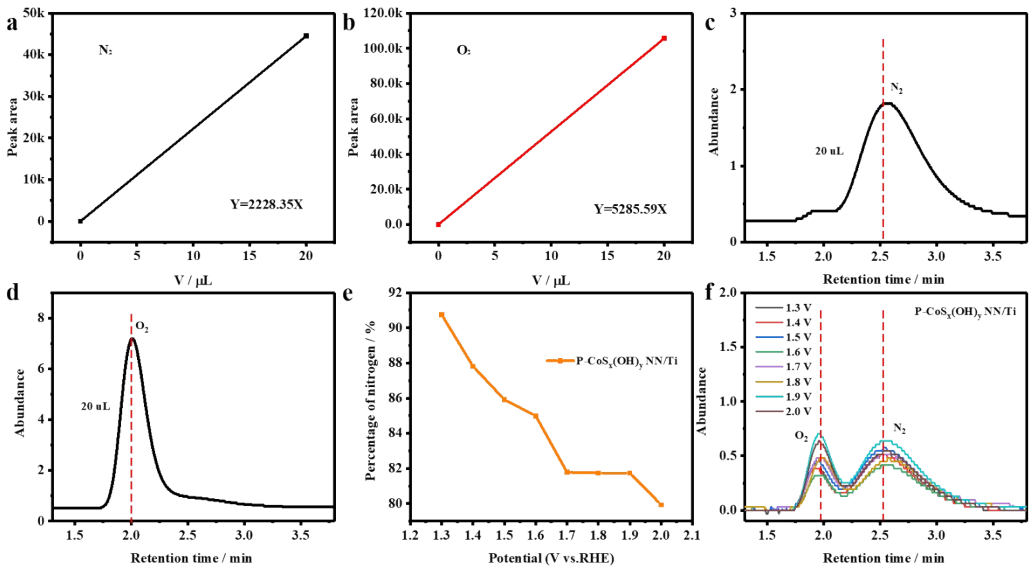

Figure S12. Standard lines of (a) nitrogen and (b) oxygen made by measuring gas volumes and corresponding measurement areas. The measured graphics of (c) nitrogen, (d) oxygen. (e)The percentage of nitrogen in the gas produced by electrolysis of 1.0 M KOH + 0.5 M urea at different potentials, and the corresponding measured graphics of (f) P-$CoS_x(OH)_y$ NN/Ti.

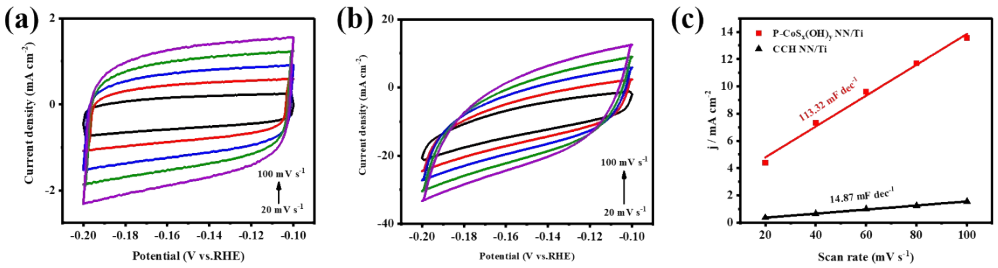

Figure S13. CV curves of (a) CCH NN/Ti, (b) P-$CoS_x(OH)_y$ NN/Ti. (c) The calculated C_{dl} for the CCH NN/Ti and P-$CoS_x(OH)_y$ NN/Ti.

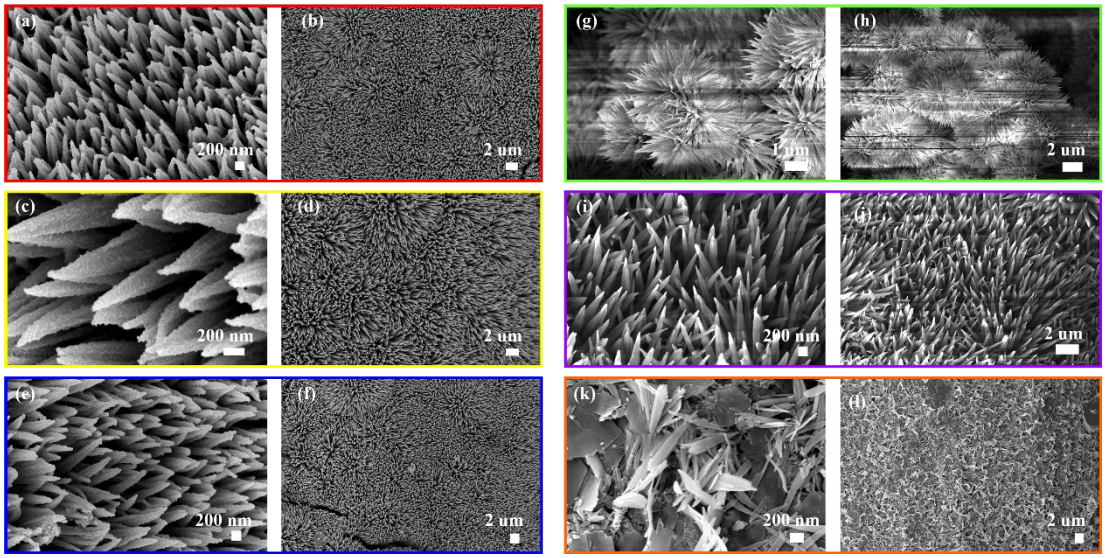

Figure S14. high magnification SEM images and low magnification SEM images of CCH NN/Ti after 1 M (a,b), 3 M (c,d), 5 M (e,f) of Na_2S treated at room temperature. high magnification SEM images and low magnification SEM images of CCH NN/Ti after 3 M Na_2S treated at 100 °C (g,h), 120 °C (i,j), 140 °C(k,l).

Table S1. The O=C−O contents of CCH NN/Ti and P-$CoS_x(OH)_y$ NN/Ti calculated from the XPS.

Samples	O=C−O
CCH NN/Ti	45.7 %
P-$CoS_x(OH)_y$ NN/Ti	13.2 %

Table S2. Comparison of the catalytic HER performance for P-$CoS_x(OH)_y$ NN/Ti with the reported catalysts in 1.0 M KOH.

Samples	η/mV @10 mA cm^{-2}	Reference
P-$CoS_x(OH)_y$ NN/Ti	86	This work
NiMnOP/NF	91	[1]
Ni@CoO@CoNC	190	[2]
NF/N-$CoMoO_4$	93	[3]
1T-WS_2	118	[4]
Ni_3N/NF	120	[5]
CoP NFs	122	[6]
$CoO_x(OH)$ films	87	[7]
CoP/ NCNHP	115	[8]
NiCoP/CC	107	[9]
Cr-doped FeNi–P/NCN	190	[10]
Co/CoP-5	253	[11]
CoS-$Co(OH)_2$@aMoS_{2+x}	140	[12]
S-CoO_x/NF	136	[13]
$(Ni_{0.33}Co_{0.67})S_2$ NWs/CC	156	[14]
CoNC@N-CNF	107	[15]
Fe-Ni@NCCNTs	202	[16]

Table S3. Comparison of the catalytic UOR performance for P-$CoS_x(OH)_y$ NN/Ti with the reported catalysts in 1.0 M KOH with different concentrations of urea.

Samples	Potential/V @10 mA cm^{-2}	Reference	Concentration of urea (mol/L)
P-$CoS_x(OH)_y$ NN/Ti	1.3	This work	0.5
Ni_3N/NF	1.34	[5]	0.5
Ni-Mo nanotube	1.36	[17]	0.1
$NiCo_2S_4$ NS/CC	1.49	[18]	0.33
NF/NiMoO-Ar	1.37	[19]	0.5
CoS_2 NA/Ti	1.59	[20]	0.3
CoMn/$CoMn_2O_4$	1.32	[21]	0.5
Ni_3N NA/CC	1.35	[22]	0.33
Ni-MOF	1.36	[23]	0.33
$Ni(OH)_2$ nanotube-NF	1.41	[24]	0.33
NiO nanosheet array	1.38	[25]	0.33
NiMo sheet array	1.37	[26]	0.33
L-MnO_2	1.37	[27]	0.5

Table S4. Comparison of the catalytic performance of P-$CoS_x(OH)_y$ NN/Ti||P-$CoS_x(OH)_y$ NN/Ti with reported catalysts for urea assisted water splitting.

Samples	Potential / V@ j (mA cm^{-2})	Urea Concentration (mol/L)	Reference
P-$CoS_x(OH)_y$ NN/Ti||P-$CoS_x(OH)_y$ NN/Ti	1.3@10	0.5	This work
Co–P/NF||Co(OH)F/NF	1.42@10	0.7	[28]
NF/NiMoO-H_2||NF/NiMoO-Ar	1.38@10	0.5	[19]
Ni-Mo nanotube||Ni-Mo nanotube	1.43@10	0.1	[17]
P-CoS_2/Ti||P-CoS_2/Ti	1.375@10	0.3	[29]
MMCN	1.55@10	0.5	[30]
CoS_2 NA/Ti||CoS_2 NA/Ti	1.59@10	0.3	[20]
CoMn/$CoMn_2O_4$	1.51@10	0.5	[21]
NiCoP/CC||NiCoP/CC	1.5@10	0.5	[9]
Ni_3N/NF||Ni_3N/NF	1.38@50	0.5	[5]
Ni_3N NA/CC||Ni_3N NA/CC	1.26@10	0.33	[22]
CoS_2-MoS_2	1.29@10	0.5	[31]

References

[1] J. Balamurugan, T.T. Nguyen, V. Aravindan, N.H. Kim, J.H. Lee, Highly reversible water splitting cell building from hierarchical 3D nickel manganese oxyphosphide nanosheets, Nano Energy 69 (2020).

[2] G. Cai, W. Zhang, L. Jiao, S.-H. Yu, H.-L. Jiang, Template-Directed Growth of Well-Aligned MOF Arrays and Derived Self-Supporting Electrodes for Water Splitting, Chem 2 (2017) 791-802.

[3] K. Chi, X. Tian, Q. Wang, Z. Zhang, X. Zhang, Y. Zhang, F. Jing, Q. Lv, W. Yao, F. Xiao, S. Wang, Oxygen vacancies engineered CoMoO4 nanosheet arrays as efficient bifunctional electrocatalysts for overall water splitting, Journal of Catalysis 381 (2020) 44-52.

[4] Q. He, L. Wang, K. Yin, S. Luo, Vertically Aligned Ultrathin 1T-WS2 Nanosheets Enhanced the Electrocatalytic Hydrogen Evolution, Nanoscale Res Lett 13 (2018) 167.

[5] S. Hu, C. Feng, S. Wang, J. Liu, H. Wu, L. Zhang, J. Zhang, Ni3N/NF as Bifunctional Catalysts for Both Hydrogen Generation and Urea Decomposition, ACS Appl Mater Interfaces 11 (2019) 13168-13175.

[6] L. Ji, J. Wang, X. Teng, T.J. Meyer, Z. Chen, CoP Nanoframes as Bifunctional Electrocatalysts for Efficient Overall Water Splitting, ACS Catalysis 10 (2019) 412-419.

[7] P.W. Menezes, C. Panda, C. Walter, M. Schwarze, M. Driess, A Cobalt-Based Amorphous Bifunctional Electrocatalysts for Water-Splitting Evolved from a Single-Source Lazulite Cobalt Phosphate, Advanced Functional Materials 29 (2019).

[8] Y. Pan, K. Sun, S. Liu, X. Cao, K. Wu, W.C. Cheong, Z. Chen, Y. Wang, Y. Li, Y. Liu, D. Wang, Q. Peng, C. Chen, Y. Li, Core-Shell ZIF-8@ZIF-67-Derived CoP Nanoparticle-Embedded N-Doped Carbon Nanotube Hollow Polyhedron for Efficient Overall Water Splitting, J Am Chem Soc 140 (2018) 2610-2618.

[9] L. Sha, J. Yin, K. Ye, G. Wang, K. Zhu, K. Cheng, J. Yan, G. Wang, D. Cao, The construction of self-supported thorny leaf-like nickel-cobalt bimetal phosphides as efficient bifunctional electrocatalysts for urea electrolysis, Journal of Materials Chemistry A 7 (2019) 9078-9085.

[10] Y. Wu, X. Tao, Y. Qing, H. Xu, F. Yang, S. Luo, C. Tian, M. Liu, X. Lu, Cr-Doped FeNi-P Nanoparticles Encapsulated into N-Doped Carbon Nanotube as a Robust Bifunctional Catalyst for Efficient Overall Water Splitting, Adv Mater 31 (2019) e1900178.

[11] Z.-H. Xue, H. Su, Q.-Y. Yu, B. Zhang, H.-H. Wang, X.-H. Li, J.-S. Chen, Janus Co/CoP Nanoparticles as Efficient Mott-Schottky Electrocatalysts for Overall Water Splitting in Wide pH Range, Advanced Energy Materials 7 (2017).

[12] T. Yoon, K.S. Kim, One-Step Synthesis of CoS-Doped β-Co(OH)2@Amorphous MoS2+xHybrid Catalyst Grown on Nickel Foam for High-Performance Electrochemical Overall Water Splitting, Advanced Functional Materials 26 (2016) 7386-7393.

[13] X. Yu, Z.-Y. Yu, X.-L. Zhang, P. Li, B. Sun, X. Gao, K. Yan, H. Liu, Y. Duan, M.-R. Gao, G. Wang, S.-H. Yu, Highly disordered cobalt oxide nanostructure induced by sulfur incorporation for efficient overall water splitting, Nano Energy 71 (2020).

[14] Q. Zhang, C. Ye, X.L. Li, Y.H. Deng, B.X. Tao, W. Xiao, L.J. Li, N.B. Li, H.Q. Luo, Self-Interconnected Porous Networks of NiCo Disulfide as Efficient Bifunctional Electrocatalysts for Overall Water Splitting, ACS Appl Mater Interfaces 10 (2018) 27723-27733.

[15] W. Zhang, J. Chu, S. Li, Y. Li, L. Li, CoN C active sites-rich three-dimensional porous carbon nanofibers network derived from bacterial cellulose and bimetal-ZIFs as efficient multifunctional electrocatalyst for rechargeable Zn–air batteries, Journal of Energy Chemistry 51 (2020) 323-332.

[16] X. Zhao, P. Pachfule, S. Li, J.R.J. Simke, J. Schmidt, A. Thomas, Bifunctional Electrocatalysts for Overall Water Splitting from an Iron/Nickel-Based Bimetallic Metal-Organic Framework/Dicyandiamide Composite,

Angew Chem Int Ed Engl 57 (2018) 8921-8926.
[17] J.-Y. Zhang, T. He, M. Wang, R. Qi, Y. Yan, Z. Dong, H. Liu, H. Wang, B.Y. Xia, Energy-saving hydrogen production coupling urea oxidation over a bifunctional nickel-molybdenum nanotube array, Nano Energy 60 (2019) 894-902.
[18] W. Zhu, M. Ren, N. Hu, W. Zhang, Z. Luo, R. Wang, J. Wang, L. Huang, Y. Suo, J. Wang, Traditional NiCo2S4 Phase with Porous Nanosheets Array Topology on Carbon Cloth: A Flexible, Versatile and Fabulous Electrocatalyst for Overall Water and Urea Electrolysis, ACS Sustainable Chemistry & Engineering 6 (2018) 5011-5020.
[19] Z.-Y. Yu, C.-C. Lang, M.-R. Gao, Y. Chen, Q.-Q. Fu, Y. Duan, S.-H. Yu, Ni–Mo–O nanorod-derived composite catalysts for efficient alkaline water-to-hydrogen conversion via urea electrolysis, Energy & Environmental Science 11 (2018) 1890-1897.
[20] S. Wei, X. Wang, J. Wang, X. Sun, L. Cui, W. Yang, Y. Zheng, J. Liu, CoS2 nanoneedle array on Ti mesh: A stable and efficient bifunctional electrocatalyst for urea-assisted electrolytic hydrogen production, Electrochimica Acta 246 (2017) 776-782.
[21] C. Wang, H. Lu, Z. Mao, C. Yan, G. Shen, X. Wang, Bimetal Schottky Heterojunction Boosting Energy-Saving Hydrogen Production from Alkaline Water via Urea Electrocatalysis, Advanced Functional Materials 30 (2020).
[22] Q. Liu, L. Xie, F. Qu, Z. Liu, G. Du, A.M. Asiri, X. Sun, A porous Ni3N nanosheet array as a high-performance non-noble-metal catalyst for urea-assisted electrochemical hydrogen production, Inorganic Chemistry Frontiers 4 (2017) 1120-1124.
[23] D. Zhu, C. Guo, J. Liu, L. Wang, Y. Du, S.Z. Qiao, Two-dimensional metal-organic frameworks with high oxidation states for efficient electrocatalytic urea oxidation, Chem Commun (Camb) 53 (2017) 10906-10909.
[24] R.-Y. Ji, D.-S. Chan, J.-J. Jow, M.-S. Wu, Formation of open-ended nickel hydroxide nanotubes on three-dimensional nickel framework for enhanced urea electrolysis, Electrochemistry Communications 29 (2013) 21-24.
[25] M.-S. Wu, G.-W. Lin, R.-S. Yang, Hydrothermal growth of vertically-aligned ordered mesoporous nickel oxide nanosheets on three-dimensional nickel framework for electrocatalytic oxidation of urea in alkaline medium, Journal of Power Sources 272 (2014) 711-718.
[26] Y. Liang, Q. Liu, A.M. Asiri, X. Sun, Enhanced electrooxidation of urea using NiMoO4·xH2O nanosheet arrays on Ni foam as anode, Electrochimica Acta 153 (2015) 456-460.
[27] <anie.201600387.pdf>.
[28] M. Song, Z. Zhang, Q. Li, W. Jin, Z. Wu, G. Fu, X. Liu, Ni-foam supported Co(OH)F and Co–P nanoarrays for energy-efficient hydrogen production via urea electrolysis, Journal of Materials Chemistry A 7 (2019) 3697-3703.
[29] Y. Jiang, S. Gao, J. Liu, G. Xu, Q. Jia, F. Chen, X. Song, Ti-mesh supported porous CoS2 nanosheets self-interconnecting net-work with high oxidation states for efficient hydrogen production via urea electrolysis, Nanoscale (2020).
[30] C. Xiao, S. Li, X. Zhang, D.R. MacFarlane, MnO2/MnCo2O4/Ni heterostructure with quadruple hierarchy: a bifunctional electrode architecture for overall urea oxidation, Journal of Materials Chemistry A 5 (2017) 7825-7832.
[31] C. Li, Y. Liu, Z. Zhuo, H. Ju, D. Li, Y. Guo, X. Wu, H. Li, T. Zhai, Local Charge Distribution Engineered by Schottky Heterojunctions toward Urea Electrolysis, Advanced Energy Materials 8 (2018).